Study of the charged gravastar model with Vaidya-Tikekar metric potential

Meghanil Sinha, S. Surendra Singh
Department of Mathematics, National Institute of Technology Manipur,
Imphal-795004, India
meghanil1729@gmail.com, ssuren.mu@gmail.com
(Submitted on 16.12.2025; Accepted on 22.03.2026)

Abstract. In this manuscript we have discussed the effects of electromagnetic fields on the isotropic spherical gravastar model with the help of Vaidya-Tikekar metric potential. Mazur and Mottola were the pioneers of the structural development of the gravastar or gravitational vacuum star. In recent decades, this gravastar model has been instrumental for posing as a potential substitute for the black hole (BH), overcoming the major issues of the event horizon and central singularity. In the interior of the gravastar, the pressure is equal to the negative energy density, building a repulsive force across the thin intermediate shell which is composed of ultra relativistic plasma fluids and with the Reissner–Nordström manifold in the exterior region. We have probed into the junction connecting the two space-time continua and also various physical properties of the shell such as energy density, proper length, total energy and entropy for this thin shell gravastar model. Our stellar model's stability has also been investigated in the manuscript.
Key words: Event horizon, central singularity, gravastar, Vaidya-Tikekar metric potential.

Introduction

The eighteenth century marks the beginning of the study of celestial objects with very high density and a gravitational pull so intense, even light is held captive by it. These objects were studied by Pierre-Simon de Laplace and John Michell. Later, these bodies in interstellar space were named Black Holes (BHs) by the American physicist John Archibald Wheeler in 1964. The structure of BHs is such that singularity occupies the innermost region, while the outer boundary is defined by the event horizon. The event horizon of a BH is the boundary beyond which nothing, including light is unable to break free from the gravitational pull, marking the point of no retrieval, upon the crossing of which, everything is held captive. The singularity at the center of a BH appears at the central point of infinite density. This point was hypothesized as the singular point where all the laws of physics collapse. The ultimate fate of a high-mass celestial body has always been a subject of fascination for astrophysicists. In the terminal stages of stellar evolution, the remnant left after the formation of a planetary nebula or the detonation of a supernova will undergo gravitational collapse if its mass exceeds approximately three solar masses. Under the influence of its own gravity, this collapse leads to the formation of a BH. White dwarfs, neutron stars, strange quark stars, electro-weak stars and gravastars are also enlisted in the list of compact objects. BH astrophysics was materialized following the discovery of quasars and other active galactic nuclei (AGN) in remote galaxies. The discovery of the X-ray binary (XRB) Cygnus X-1 uplifted the above research. Karl Schwarzschild found a simple BH solution in the context of Einstein field equations in space which is regarded as the key solution in the case of a classical BH (static and uncharged). But the solution has certain limitations because of $< i >$ the occurrence of the event horizon and $< ii >$ the emergence of singularity which resulted in significant unresolved problems.

Thus it was necessary to develop a solution to deal with these challenges. In the year 2001, Mazur and Mottola developed a theoretical framework to encounter these key obstacles in the development of the BH theory, the gravitational vacuum condensate star (gravastar) (Mazur & Mottola [2001, 2004]). The most fascinating facet during the building process of the gravastar is that it demanded exact solutions which are regular at the core. Mazur and Mottola extended the research of condensation of particles at low temperature, the Bose-Einstein condensation in the gravitational system. At a temperature below normal, there must have occurred a phase transition offering a repulsive de-Sitter core preventing the formation of the event horizon and hence singularity (Gliner [1966]; Chapline et al. [2003]). In the collapse dynamics of the Mazur and Mottola framework, quantum vacuum fluctuations are anticipated to perform a pivotal role (Abramowicz et al. [2002]; Mielke & Schunck [2000]; Stephens et al. [1994]; Berezin [2003]). Leveraging this, they engineered the hypothetical, cold, compact and dark object overcoming the hurdles of central singularity and the event horizon of BH. It serves as the viable alternative to the concept of the BH. The gravitational vacuum star model fulfills all the theoretical requirements making it a stable culmination of the stellar development and delivers a solution to the issues of the classical black hole (CBH) theory. Although the observational evidence is insufficient to justify the existence of gravastar, it is crucial to analyze the gravastar framework that can be claimed as a credible choice to fix the theoretical challenges in deciphering BHs.

The different equations of state (EoS) characterizing the three regions of the gravastar are
$< i >$ interior $(0 \leq r < r_1) : p = -\rho$
$< ii >$ shell $(r_1 \leq r \leq r_2) : p = \rho$
$< iii >$ exterior $(r_2 < r) : p = \rho = 0$,
where the radius of the transition shell is in the vicinity of $r_1 < r < r_2$, with $r_1 \equiv D$ and $r_2 \equiv D + \epsilon$ with $\epsilon \ll 1$, and r_1 and r_2 denotes the radius of the interior and the outer region of the gravastar respectively. The interior region of the gravastar portrays the dark energy scenario (or vacuum energy) with negative matter energy density generating the repulsive phenomenon across the shell radiating outward from the center of the model (i.e. $r = 0$). In a different vein, the shell having the positive matter energy density provides the required gravitational pull to offset the repulsive effect from the interior.

To ensure the stability of gravastar, their dynamical stability was analyzed (Visser & Wiltshire [2004]). Mazur and Mottola's five layered construction of the gravastar was reduced to three layers by Visser & Wiltshire [2004]. The EoS for the thin shell indicates a stiff fluid pertaining to the cold baryonic Universe (Zel'dovich [1972]). The stability of the gravastar alongside the manifestation of the thin shell has been probed into, where the Israel junction condition is in accordance for the purpose of joining de-Sitter spacetime (interior) with the Reissner–Nordström (exterior) metric (Carter [2005]). Analysis of the EoS parameter was also done in the realm of the gravastar framework. The exact solutions for the spherically symmetric spacetime amidst electric charge were found, by additionally analyzing the discoveries with the existing BHs (de Felice et al. [1995]). Consequently, it can be inferred that the effect of electric charge can mitigate the occurrence of gravitational collapse to a considerable extent. The quest for an exact solution of the Einstein field

equations for static isotropic and anisotropic interstellar objects make an ideal testing ground which fascinates mathematicians as well as physicists. Nevertheless, the majority of the solutions fall short of the essential physical conditions of the stellar systems. Thus, explicit solutions for the Einstein-Maxwell field equations were essential in relativistic astrophysics. Although Einsteins's General Relativity (GR) holds great potential to uncover most of the significant mysteries of nature, later it was acknowledged that its refinement was necessary. The Einstein field equations came into view in the year of 1915, demonstrating how local spacetime curvature is linked to the gravitational field (Einstein [1915]). In the same way, the Einstein-Maxwell equations combined the principles of GR (as described by Einstein's field equations) and electromagnetism (from Maxwell's equations), unifying the curvature of local spacetime and electromagnetic field. We have available many solutions in the case of field equations, the Schwarzschild solution which outlined gravitational fields (Schwarzschild [1916]), the Reissner-Nordström solution which categorized a gravitational electromagnetic field (Carmeli [1982]), Kerr's solution that described gravitational fields with rotational motion and the Kerr-Newman solution of electromagnetic fields in rotation (Islam [1985]). The GR theory laid the foundation to usher in a new era of mathematical physics.

The simplest known approach in the case of a statically charged perfect fluid solution regarding compact objects is intended through a metric ansatz or an EoS in relation to pressure and density. A class of charged compact stellar models with anisotropic pressure was developed in the work of Maurya & Govender [2017], where exact solutions of the Einstein-Maxwell field equations were obtained and their physical viability was analyzed. The gravitational decoupling approach has been successfully applied to construct physically viable charged compact stellar configurations (Maurya et al. [2019]). Moreover, charged compact stellar configurations generated through the gravitational decoupling method have been investigated (Maurya [2020]). The effects of torsion-matter coupling gravity on charged compact stars have also been explored (Maurya et al. [2024]). Furthermore, charged stellar structures have also been studied in modified extended theories (Ilyas et al. [2023]). Their formation was studied and the mass-radius relations in the lower mass gap region has been analyzed (Maurya et al. [2025]). In the current analysis to resolve the field equations, we have utilized the Vaidya-Tikekar metric potential depending upon the parameter K, an ansatz for in terms of the spatial arrangement $t =$ constant hyper-surface (Vaidya & Tikekar [1982]). The most significant characteristic is that the solution provides a collection of static spherically symmetric perfect fluid configuration and affords an exact solution of field equations. In this context, we have taken into account $K \notin [0, 1]$, for charged perfect fluid model. Charged compact stellar configurations have also been investigated in modified gravity frameworks based on geometrical ansatz like the Vaidya-Tikekar stellar model (Maurya et al. [2023]). In modified gravity approaches, it has also been employed to investigate stellar stability and mass limits (Lohakare et al. [2022]). Furthermore, the influence of electric charge on compact stellar configurations has also been explored within the Vaidya-Tikekar framework (Kumar et al. [2018]). Apart from the Vaidya-Tikekar stellar model, several other non-singular metric potentials have also played a significant role in the modeling of realistic compact stellar configurations. In particular, the Durgapal-Fuloria metric potential and the Tolman-

Kuchowicz metric potential have been widely employed to construct physically viable interior solutions describing relativistic stars. These metric potentials are especially useful because they yield regular and well-behaved solutions for the gravitational field equations, ensuring finite values of physical quantities such as pressure, density, and metric functions throughout the stellar interior. Consequently, they have been extensively applied in the study of compact objects within various theoretical frameworks including GR and beyond (Gupta & Maurya [2011]; Maurya et al. [2015]; Biswas et al. [2019]; Maurya & Tello-Ortiz [2020a]; Maurya & Tello-Ortiz [2020b]; Errehymy & Daoud [2021]; Maurya et al. [2022]; Maurya et al. [2023]; Rej et al. [2023]; Bhar et al. [2024]). Their ability to generate singularity-free solutions satisfying energy conditions and stability criteria makes them valuable tools for investigating the internal structure and physical properties of highly dense astrophysical objects. Further, we can also see complexity-free anisotropic compact stellar solution in modified gravity backdrop using the gravitational decoupling technique (Maurya et al. [2023]). Moreover, anisotropic compact star models using the embedding class-I approach in GR were studied and their physical viability and stability were analyzed (Errehymy et al. [2021]). The complexity formalism combined with the MGD approach has also been applied to analyze anisotropic compact stars in modified gravity theories (Maurya et al. [2023]). Stable self-gravitating anisotropic configurations based on a modified Van der Waals EoS were also investigated (Errehymy et al. [2022]).

After the concept of the gravastar has come into existence, many researchers have been involved in revealing its secrets in different modified theories of gravity as well as in different spacetimes. In the literature we can see the structure of gravastars in modified theories such as $f(R,T)$ (Das et al. [2017]), $f(R,G)$ (Bhatti et al. [2020]), Rastall gravity (Ghosh et al. [2021]), $f(R,\Sigma,T)$ (Shafeek et al. [2023]), $f(Q)$ (Pradhan et al. [2023]) and $f(Q,T)$ (Pradhan et al. [2023]) gravity. In different dimensional space-time gravastars have been a subject of fascination to many researchers (Rahaman et al. [2012]; Övgün et al. [2017]; Bhattacharjee et al. [2023]). Further charged gravastars in different gravities as well as different space-times featuring the exterior Schwarzschild geometry substituted by Reissner–Nordström space-time continuum is available at the references (Ghosh et al. [2017]; Debnath [2019]; Yousaf et al. [2019]; Bhatti [2020]; Debnath [2021]; Mohanty et al. [2023], Mohanty et al. [2024]; Mustafa et al. [2024]; Bhattacharjee & Chattopadhyay [2024]). Researchers have extensively explored gravastar configurations using different non-singular metric potentials in modified frameworks to understand their internal structure, stability conditions, and physical properties. These studies aim to construct well-behaved interior solutions that remain free from central singularities while satisfying all physical requirements (Ghosh et al. [2020]; Sinha & Singh [2025a, 2025b]). Recently gravastars in the light of conformal motion have also been probed into Sharif & Waseem [2019], Sharif & Saeed [2022], Sanjay et al. [2024].

The main concern of this paper is the exploration of gravastars using the Vaidya-Tikekar metric potential which provides a non-singular solution to the gravastar model overcoming the issues of the CBH theory. The blueprint of the proposed work is as follows: Section 1 deals with the composition of the gravastar model with the help of Vaidya-Tikekar metric potential in the realm

of Einstein-Maxwell field equations. Section 2 focuses on the interior geometry of the gravitational vacuum condensate star, with Sect. 3 addressing the shell region along with its various physical features. Section 4 pertains to the Reissner-Nordström geometry in the exterior periphery of the gravastar. Section 5 talks about the junction condition following the EoS parameter. In Sect. 6 we discuss the stability analysis and the paper wraps up with a discussion and concluding remarks in the Conclusion section.

1. Field equation in the realm of Vaidya-Tikekar metric potential

In order to study gravastars, we have taken into account the spacetime of an isotropic spherical matter configuration in the form

$$ds^2 = e^{x(r)}dt^2 - e^{y(r)}dr^2 - r^2(d\theta^2 + \sin^2\theta d\phi^2), \tag{1}$$

where the metric potentials are functions of the radial parameter r. The field equation for the hydrostatic stellar structure in the case of a charged sphere is given by

$$-\kappa(T_j^i + E_j^i) = R_j^i - \frac{1}{2}R\delta_j^i = G_j^i, \tag{2}$$

where $\kappa = \frac{8\pi G}{c^4}$, G signifies the gravitational constant and c indicates the speed of light, R_j^i symbolizes the Ricci tensor with R as the Ricci scalar respectively. In the entire manuscript, it has been presupposed that $G = c = 1$. T_j^i is the energy-momentum tensor and E_j^i indicates the electromagnetic field tensor. A key issue comes to the fore regarding the distribution of matter inside the star is that in this analysis we have looked at the scenario involving an object with both gravitational mass and electric charge having isotropic pressures. Here, we have presumed perfect fluid with the energy momentum tensor as

$$T_{\mu\nu} = (\rho + p)U_\mu U_\nu - pg_{\mu\nu}, \tag{3}$$

where ρ and p indicate the density and pressure respectively and U_ν the four-velocity vector. The electromagnetic field tensor is formulated as

$$E_{\alpha\beta} = \frac{1}{4\pi}(F_\alpha^\gamma F_{\beta\gamma} - \frac{1}{4}F^{\gamma\eta}F_{\gamma\eta}g_{\xi\alpha}). \tag{4}$$

The Maxwell-field tensor is given by the four potential Ψ_α as

$$F_{\alpha\beta} = \Psi_{\beta,\alpha} - \Psi_{\alpha,\beta} \tag{5}$$

satisfying the conditions

$$F_{ik,j} + F_{kj,i} + F_{ji,k} = 0 \tag{6}$$

and we have also

$$[\sqrt{-g}F^{\alpha\beta}]_{,\beta} = 4\pi J^\alpha\sqrt{-g}\,. \tag{7}$$

Here, J^{α} depicts the electromagnetic four-current density with $J^{\alpha} = \sigma U^{\alpha}$, where σ is the charge density. The electric intensity E is outlined by virtue of electric charge q as

$$E = \frac{q}{r^2}\,. \tag{8}$$

We generate a range of field equations from the Einstein-Maxwell equation as

$$\frac{e^{-y}}{r^2}(-1 + e^{y} + y^{'}r) = 8\pi\rho + E^2 \tag{9}$$

$$\frac{e^{-y}}{r^2}(-1 + e^{y} - x^{'}r) = -8\pi p + E^2 \tag{10}$$

$$\frac{e^{-y}}{4r}[2(y^{'} - x^{'}) + (2x^{''} + x^{'2} - x'y')r] = 8\pi p + E^2. \tag{11}$$

Due to the presence of five unknown quantities $x, y, \rho(r), p(r)$ and $E(r)$ in terms of three equations (9)–(11) with its complex characteristics and non-linearity, it is difficult to solve. Consequently, we assume the commonly known Vaidya-Tikekar metric potential here as

$$e^{x(r)} = \frac{K(1 + Cr^2)}{K + Cr^2}, \quad \text{for } K \notin (0, 1), \tag{12}$$

where C and K are the constant parameters. This preference of metric potential gives access to singularity free solution at $r = 0$ and $e^{y(0)} = 1$. This metric potential has been used to analyze spheroidal spacetimes in the context of compact and super-dense stars. For studying charged gravastar configurations in GR, the adoption of the Vaidya-Tikekar metric potential for the temporal metric component provides advantages. The adopted form significantly simplifies the coupled equations governing the charged gravitating system here. This specific ansatz reduces the complexity of the field equations and facilitates the derivation of exact or tractable analytic solutions for the interior spacetime. Physically, the Vaidya-Tikekar geometry represents a spheroidal spatial hypersurface embedded in a higher-dimensional flat space, allowing the parameter K to control the deviation from perfect spherical geometry and thereby regulate the density distribution of the stellar configuration. The constants provide flexibility to model realistic matter distributions while ensuring that the metric functions remain finite and well behaved at the center which guarantees regular pressure and energy density, which is an essential requirement for physically acceptable compact objects. From an observational standpoint, this metric form also allows the calculation of measurable quantities such as surface gravitational redshift which can be compared with observational constraints obtained from compact stars and high energy astrophysical observations. Moreover, the chosen form allows the interior gravastar region to be smoothly matched, through appropriate junction conditions. Therefore, the Vaidya-Tikekar potential not only provides mathematical tractability in solving the field equations but also offers a flexible and observationally testable framework for analysing the internal structure and observable characteristics

of highly compact astrophysical objects. Subsequent to mathematical arrangements, we arrive at the following equations from equations (9)–(11) with the help of this metric potential as (Vaidya & Tikekar [1982])

$$-\frac{e^{-y}}{r^2}+\frac{1}{r^2}+\frac{e^{-y}y'}{r}=8\pi\rho+E^2 \tag{13}$$

$$-\frac{e^{-y}}{r^2}+\frac{1}{r^2}+\frac{Ce^{-y}(K-1)}{(K+Cr^2)(1+Cr^2)}=-8\pi p+E^2 \tag{14}$$

$$\begin{aligned}\frac{e^{-y}}{4r}\Bigg[&2y'-\frac{2CKr}{K(1+Cr^2)}-\frac{2Cr}{K+Cr^2}\\&-\frac{8C^2r^3}{(1+Cr^2)^2}+\frac{4Cr}{1+Cr^2}+\frac{8C^2r^3}{(K+Cr^2)^2}-\frac{4Cr}{K+Cr^2}\\&+\left(\frac{2CKr}{K(1+Cr^2)}-\frac{2Cr}{K+Cr^2}\right)^2 r\\&-\left(\frac{2CKr^2}{K(1+Cr^2)}-\frac{2Cr^2}{K+Cr^2}\right)y'\Bigg]=8\pi p+E^2.\end{aligned} \tag{15}$$

From the above equations, we can study the charged fluid distribution for $K<0$ and $K>1$. The energy conservation equation is given by

$$\frac{x'}{2}(\rho+p)+\frac{dp}{dr}=\frac{1}{8\pi r^4}(r^4E^2)'\,. \tag{16}$$

2. Interior spacetime of gravastar

Gravastars comprise of three regions distinguished by the EoS $p=\omega\rho$ for different values of ω where $\omega=$constant (Mazur & Mottola [2001, 2004]). In this section we focus on the internal structure of a star that is filled with an obscure gravitational presence accompanied by the EoS in the context of dark energy as

$$p=-\rho\Longrightarrow\omega=-1. \tag{17}$$

The centre-emitting negative/repulsive pressure is in the radially outward direction for the spherically symmetric configuration of the gravitating bodies to counteract the inward gravitational pull. The above EoS is labeled as a "degenerate vacuum" or "$\rho-vacuum$" (Davies [1984]; Blome & Priester [1984]; Hogan [1984]; Kaiser & Stebbins [1984]). In the gravastar framework, the interior region is commonly described by the above EoS for the vacuum energy dominated or de-Sitter type spacetime. This assumption originates from the pioneering works of Mazur & Mottola [2001, 2004] in their proposal of gravitational vacuum condensate stars (gravastars), where they suggested that gravitational collapse may lead to a phase transition of spacetime rather than the

formation of a CBH singularity. In this picture, the interior of the gravastar is filled with a form of vacuum energy characterized by the EoS $p = -\rho$, which is identical to the associated cosmological constant in GR. Such an EoS produces a repulsive gravitational effect. As a result, the interior region behaves like a de-Sitter spacetime with constant energy density, preventing further gravitational collapse and eliminating the possibility of a central curvature singularity. Physically, this configuration can be interpreted as a gravitational vacuum condensate, representing a quantum vacuum phase of spacetime that forms when the collapsing matter reaches extremely high densities. In addition to its theoretical motivation, the EoS has a natural connection with dark energy in cosmology, where observational evidence suggests that the EoS parameter is close to -1. Consequently, the gravastar interior may be viewed as a localized region of dark energy-like vacuum. This assumption ensures a regular interior solution and facilitates a smooth matching with the surrounding thin shell and the exterior geometry, thereby forming a stable compact object without an event horizon or singularity. The use of this EoS in gravastar models has been extensively discussed in the works of Visser & Wiltshire [2004], Chirenti & Rezzolla [2007], Ray et al. [2020]. Putting $p = -\rho$ into the conservation equation, we get

$$p = -\rho = -\rho_l \quad \text{(constant)}. \tag{18}$$

We consider E as $E = \varkappa r^m$ where m is a non-negative constant and $\varkappa$ is free from r (Debnath [2019, 2021]). Using this into the equation (13), we get

$$e^{-y} = 1 - \frac{8\pi\rho_l r^2}{3} + \frac{\varkappa^2 r^{2m+2}}{2m+3} + \frac{A}{r}\,, \tag{19}$$

where A is the integration constant. For the gravastar which has no singularities at the center, we take $A = 0$ (Yousaf et al. [2019]). Accordingly, we get the metric potential as

$$e^{-y} = 1 - \frac{8\pi\rho_l r^2}{3} + \frac{\varkappa^2 r^{2m+2}}{2m+3}\,. \tag{20}$$

And also to avoid singularities, we must have $\frac{8\pi\rho_l r^2}{3} + \frac{\varkappa^2 r^{2m+2}}{2m+3} \neq 1$ and $2m \neq -3$. For the matter density which remains constant throughout the entirety of the interior region, we can determine the active gravitational mass as

$$M(D) = \int_0^{r=D} 4\pi r^2 \Big(\rho_l + \frac{E^2}{8\pi}\Big) dr = \frac{4\pi D^3 \rho_l}{3} + \frac{\varkappa^2 D^{2m+3}}{2(2m+3)}\,. \tag{21}$$

The preceding equation reveals that the gravitational mass enclosed within the interior of the stellar structure is in direct proportion to the radial co-ordinate. This is a distinctive characteristic of the dense celestial body. In addition, the above mentioned equation also describes the significant reliance of the mass on the specific value $r = D$ due to the existence of electric charge. The integral is no longer finite upon the substitution of $r = \infty$. Nevertheless, this selection is not viable, as it's not feasible to consider the limitless dimension of the stellar body.

3. Intermediate thin shell

In the below section, we discuss the consequences of electromagnetic interactions in the process of constructing the intermediate shell of the gravastar. Here, we take into account that the shell is formed of an ultra-relativistic perfect fluid with a high degree of compactness obeying the EoS $p = \rho$. Pertaining to the cold baryonic Universe, Zel'dovich initiated the concept of this type of fluid. Numerous authors have thoroughly investigated this type of fluid to investigate diverse perspectives of cosmic evolution including astrophysical phenomena (Carr [1975]; Madsen et al. [1992]; Chakraborty & Pradhan [2001]; Buchert [2001]; Braje & Romani [2002]; Linares et al. [2004]). For a non-vacuum region, it is extremely challenging to acquire a general solution of the field equation. To circumvent this issue, we will employ an approximation $0 < e^{-y} \leq 1$. For r approaching 0, any r-dependent parameter can be considered $\ll 1$. From the above assumptions and with the help of equations (13) and (14), we get

$$e^{y(r)} = \frac{B_1}{2(1+m)} \times \Big(-2\varkappa^2 r^{2m+2} - 4(1+m)\log(r) \\ -(1+m)\log(-K - Cr^2) + \log(1+Cr^2) + m\log(1+Cr^2)\Big). \quad (22)$$

Here B_1 is serving as the integration constant. We have considered E as

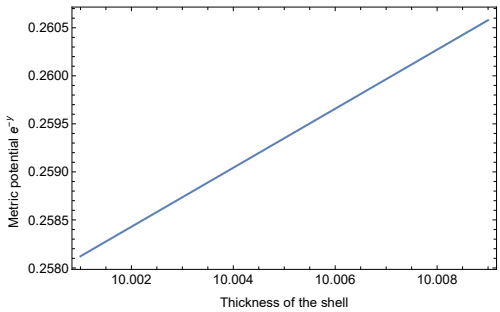

Fig. 1. Variation of the metric potential $e^{-y(r)}$ in the shell with respect to the shell thickness (ϵ) for $B_1 = 0.01$.

$E = \varkappa r^m$ as the function of r where m is a non-negative constant and $\varkappa$ is independent from r. From the conservation equation (16), we derive the expression for pressure as

$$p = \rho = e^{\frac{(-1+K)K}{K+Cr^2}} \Big(J - \frac{e^{-\frac{(-1+K)K}{K+Cr^2}}(-\varkappa^2 K^2 r^{2m} - 2C\varkappa^2 K r^{2+2m} - C^2\varkappa^2 r^{4+2m})}{8\pi(K+Cr^2)^2} \Big) \quad (23)$$

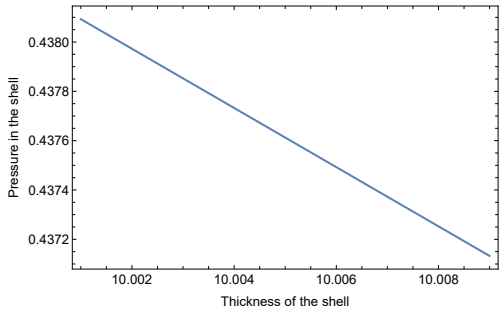

Fig. 2. Plot of pressure in the shell with respect to the shell thickness (ϵ).

where J is a constant. Figs. 1 and 2 show the variation of the metric potential $e^{-y(r)}$ and that of pressure or matter density as the thickness parameter varies in the shell, and how it stays positive in this region. The metric potential shows a smooth and stable solution here and the pressure decreases outwards in the shell (Naz & Sharif [2022]; Pradhan et al. [2023]), for the model of HER X-1 for $K = -1.313519$ and $C = 0.003078799$ (Gupta & Maurya [2011]). In the shell region of our stellar model, we can see the nature of the inverse of the radial metric component in Fig. 1, which characterizes the radial geometric structure of spacetime inside the thin shell. Clearly, $e^{-y(r)}$ increases monotonically with the shell thickness and remains smooth without any singularities, indicating that the radial spacetime geometry is well-behaved throughout the shell region. Physically, this behavior implies that the interior gravitational field varies smoothly and that the shell does not develop any pathological features such as divergences or horizons within its extent. The monotonic increase further suggests a gradual and stable transition of the spacetime curvature from the interior region of the gravastar towards the exterior, ensuring that the metric functions remain finite and continuous across the shell. Such regular and non-singular behavior of the metric potential is generally regarded as a necessary condition for a physically acceptable and stable gravastar configuration. We can also see that both pressure and energy density decrease smoothly and monotonically across the shell without any singularities, which indicates that the shell matter is distributed in a physically regular and stable manner. A smooth decrease means that the internal stresses gradually diminish from the inner boundary of the shell toward the outer boundary, avoiding abrupt changes or divergences in the matter variables. Physically, this reflects a well-behaved stiff matter layer that supports the gravastar structure by providing sufficient pressure to counterbalance gravitational attraction while maintaining its behavior. The absence of singularities further implies that the shell configuration is free from discontinuous behavior and allows for a continuous and smooth matching and thus reinforcing the viability of the thin shell gravastar model.

3.1. Proper length of the shell

The thin shell is matched with the interior at $r = D$ to the exterior at $r = D+\epsilon$. It is assumed to be very small as $0 < \epsilon \ll 1$. Following the proposed theoretical structure of Mazur and Mottola's, the rigid fluid in the shell lies in between the junction of two spacetimes. The dimension of the shell extends from $r = D$ (i.e. the interface between the interior and the intermediate shell) to $r = D+\epsilon$ (the interface between the shell and the exterior space-time). It can be expressed using equation (22) in mathematical terms as

$$\begin{aligned}\ell &= \int_D^{D+\epsilon} \sqrt{e^{y(r)}}dr \\ &= \Big[\frac{\sqrt{B_1}}{2(1+m)}\Big(4(1+m)r - \frac{2\varkappa^2 r^{3+2m}}{3+2m} + \Big(2+2m\Big)\Big(\frac{\arctan[\sqrt{C}r]}{\sqrt{C}}\Big) \\ &\quad -\Big(2\sqrt{K}+2\sqrt{K}m\Big)\Big(\frac{\arctan[\frac{\sqrt{C}r}{\sqrt{K}}]}{\sqrt{C}}\Big) - 4(1+m)r\log[r] - r\log[-K-Cr^2] \\ &\quad -mr[-K-Cr^2] + r\log[1+Cr^2] + mr\log[1+Cr^2]\Big)\Big]_D^{D+\epsilon}. \end{aligned} \tag{24}$$

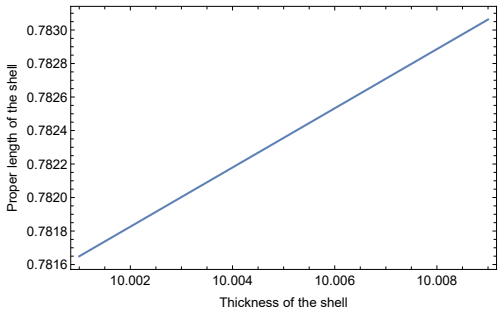

Fig. 3. Graph of the proper length of the shell with respect to the shell thickness (ϵ).

From Fig. 3, the proper length is observed to increase as the shell thickness grows (Debnath [2021]; Pradhan et al. [2023]), for the model HER X-1 for $K = -1.313519$ and $C = 0.003078799$ (Gupta & Maurya [2011]). The proper length also shows smooth nature with the shell thickness and exhibits no singularities, which indicates that the radial geometry of spacetime inside the shell is regular throughout the region. Physically, this smooth and monotonic behavior implies that the shell matter is distributed in a stable and continuous manner. It also suggests that the spacetime structure within the shell undergoes a gradual geometric transition from the interior gravastar core to the exterior metric, confirming that the shell forms a physically acceptable

layer with finite thickness and consistent gravitational properties. Such regular behavior of the proper length is an important indicator of the viability and stability of the gravastar configuration.

3.2. Energy

We presume the EoS ($p = -\rho$) for the interior section that demonstrates the zone embodying a negative energy and endorse the repulsive properties of the interior sector. But the energy contained within the shell is given by

$$\mathtt{E} = \int_D^{D+\epsilon} 4\pi\rho r^2 dr = 4\pi \int_D^{D+\epsilon} \Big[r^2 e^{\frac{(-1+K)K}{K+Cr^2}} \times \Big(J - \frac{e^{-\frac{(-1+K)K}{K+Cr^2}} (-\varkappa^2 K^2 r^{2m} - 2C\varkappa^2 K r^{2+2m} - C^2\varkappa^2 r^{4+2m})}{8\pi(K+Cr^2)^2} \Big) \Big] dr. \quad (25)$$

Owing to the difficulty of the integral's analytical solution, we assume

$$\Big[r^2 e^{\frac{(-1+K)K}{K+Cr^2}} \Big(J - \frac{e^{-\frac{(-1+K)K}{K+Cr^2}} (-\varkappa^2 K^2 r^{2m} - 2C\varkappa^2 K r^{2+2m} - C^2\varkappa^2 r^{4+2m})}{8\pi(K+Cr^2)^2} \Big) \Big] = \frac{dn(r)}{dr}.$$

As the shell is very thin, $\epsilon \ll 1$, we can have $O(\epsilon^2) \approx 0$. From the Taylor series expansion and by restricting ourselves up to the first order term of ϵ, from the above integral we can have

$$\begin{aligned} \mathtt{E} &= 4\pi \int_D^{D+\epsilon} \frac{dn(r)}{dr} dr = 4\pi[n(D+\epsilon) - n(D)] \\ &\approx 4\pi\epsilon \frac{dn(r)}{dr}\Big|_D \approx 4\pi\epsilon \Big[r^2 e^{\frac{(-1+K)K}{K+CD^2}} \Big(J - \\ &\quad \frac{e^{-\frac{(-1+K)K}{K+CD^2}} (-\varkappa^2 K^2 D^{2m} - 2C\varkappa^2 K D^{2+2m} - C^2\varkappa^2 D^{4+2m})}{8\pi(K+CD^2)^2} \Big) \Big]. \quad (26) \end{aligned}$$

Clearly the energy of the shell depends on the shell thickness here whose nature can be interpreted from Fig. 4 for $K = -1.313519$ and $C = 0.003078799$ and $\epsilon = 0.001$. From the figure it can be observed that the energy rises as the shell's thickness increases. It meets the requirement that the energy of the shell must be increased with the radial distance (Pradhan et al. [2023]). The energy contained in the shell represents the total matter-energy contribution of the stiff fluid layer separating the interior core from the exterior region. The nature of the energy of the shell indicates that a thicker shell contains a larger amount of matter-energy distributed over the radial extent of the shell region. This behavior reflects the accumulation of energy density across the shell with its radial width, implying that the shell acts as the primary region where the gravastar stores its mass-energy. Such an increasing trend is physically reasonable because a larger shell volume accommodates more matter and electromagnetic contribution, leading to a higher total energy content.

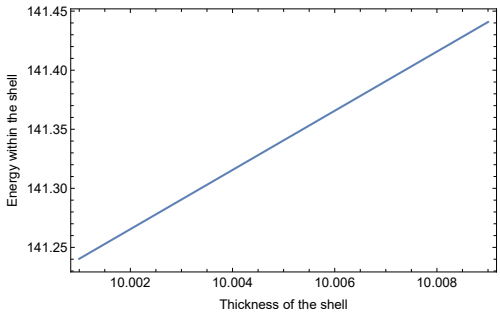

Fig. 4. Plot of energy within the shell with respect to the shell thickness (ϵ).

The smooth increase of energy with thickness therefore supports the idea of a stable and well-distributed matter configuration within the shell, contributing to the overall gravitational structure of the gravastar without introducing singular or unphysical behavior.

3.3. Entropy

Entropy indicates the disorderness inside the gravastar. Mazur and Mottola recommended zero entropy within the interior region of the gravastar that remains stable under a specific condensed phase. But the entropy relation is computable within the shell through the given formula as

$$S = \int_{D}^{D+\epsilon} 4\pi\, r^2 s(r) \sqrt{e^{y(r)}} dr\,, \tag{27}$$

where $s(r)$ is entropy of the local temperature $T(r)$ which is determined by

$$s(r) = \frac{\eta^2 k_B^2 T(r)}{4\pi\hbar^2} = \eta \left(\frac{k_B}{\hbar}\right) \sqrt{\frac{p}{2\pi}}\,, \tag{28}$$

where η is a dimensionless constant. We use geometrical ($G = c = 1$) as well as Planckian ($k_B = \hbar = 1$) units in our manuscript. Thus, we get

$$s(r) = \eta \sqrt{\frac{p}{2\pi}}\,. \tag{29}$$

Using equation (29) in equation (27), we can get the entropy as

$$
\begin{aligned}
S &= \int_D^{D+\epsilon} 4\pi\, r^2 \eta \sqrt{\frac{p}{2\pi}} \sqrt{e^{y(r)}}\, dr \\
&= 2\sqrt{2}\sqrt{\pi}\sqrt{B_1}\eta \int_D^{D+\epsilon} r^2 \times \\
&\quad \sqrt{e^{\frac{(-1+K)K}{K+Cr^2}} \Big(J - \frac{e^{-\frac{(-1+K)K}{K+Cr^2}} (-\varkappa^2 K^2 r^{2m} - 2C\varkappa^2 K r^{2+2m} - C^2\varkappa^2 r^{4+2m})}{8\pi(K+Cr^2)^2}\Big)} \times \\
&\quad \Big(\frac{1}{2(1+m)} \times \Big(-2\varkappa^2 r^{2m+2} - 4(1+m)\log(r) - (1+m)\log(-K-Cr^2) \\
&\quad + \log(1+Cr^2) + m\log(1+Cr^2)\Big)\Big)^{\frac{1}{2}} dr\,. \qquad (30)
\end{aligned}
$$

By assuming

$$
\frac{dh(r)}{dr} = r^2 \times \sqrt{e^{\frac{(-1+K)K}{K+Cr^2}} \Big(J - \frac{e^{-\frac{(-1+K)K}{K+Cr^2}} (-\varkappa^2 K^2 r^{2m} - 2C\varkappa^2 K r^{2+2m} - C^2\varkappa^2 r^{4+2m})}{8\pi(K+Cr^2)^2}\Big)} \times
$$
$$
\Big(\frac{1}{2(1+m)} \times \Big(-2\varkappa^2 r^{2m+2} - 4(1+m)\log(r) - (1+m)\log(-K-Cr^2) + \log(1+
$$
$$
Cr^2) + m\log(1+Cr^2)\Big)\Big)^{\frac{1}{2}}.
$$

Since $\epsilon \ll 1$, thus $O(\epsilon^2) \approx 0$, hence we get from the Taylor series expansion by restricting ourselves up to the first order term of ϵ

$$
\begin{aligned}
S &= 2\sqrt{2}\sqrt{\pi}\sqrt{B_1}\eta \int_D^{D+\epsilon} \frac{dh(r)}{dr} dr = 2\sqrt{2}\sqrt{\pi}\sqrt{B_1}\eta[h(D+\epsilon) - h(D)] \\
&\approx 2\sqrt{2}\sqrt{\pi}\sqrt{B_1}\eta\epsilon \frac{dh(r)}{dr}\,|_D \\
&\approx 2\sqrt{2}\sqrt{\pi}\sqrt{B_1}\eta\epsilon D^2 \times \\
&\quad \sqrt{e^{\frac{(-1+K)K}{K+CD^2}} \Big(J - \frac{e^{-\frac{(-1+K)K}{K+CD^2}} (-\varkappa^2 K^2 D^{2m} - 2C\varkappa^2 K D^{2+2m} - C^2\varkappa^2 D^{4+2m})}{8\pi(K+CD^2)^2}\Big)} \times \\
&\quad \Big(\frac{1}{2(1+m)} \times \Big(-2\varkappa^2 D^{2m+2} - 4(1+m)\log(D) - (1+m)\log(-K-CD^2) \\
&\quad + \log(1+CD^2) + m\log(1+CD^2)\Big)\Big)^{\frac{1}{2}}. \qquad (31)
\end{aligned}
$$

We get the entropy which is directly proportional to the thickness ϵ of the shell and it also depends on $\varkappa$. The variation of the entropy within the shell is depicted in Fig. 5 for $K = -1.313519$ and $C = 0.003078799$ and $\epsilon = 0.001$. Thus we can see that the entropy reaches a maximum towards the outer boundary of the shell which indicates a stable stellar configuration under this structural framework (Das et al. [2017]; Debnath [2021]; Pradhan et al. [2023]). The entropy of the shell represents the measure of thermodynamic degrees of freedom associated with the matter distribution in the shell. As the entropy increases proportionally with the shell thickness, it physically

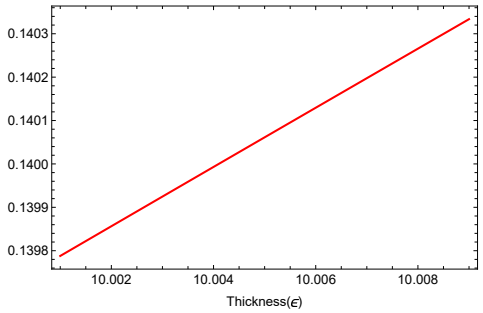

Fig. 5. Variation of the entropy of the shell with respect to the shell thickness (ϵ).

indicates that the thermodynamic content of the shell grows steadily as the radial extent of the shell increases. This behavior suggests that the shell matter contributes uniformly to the thermodynamic structure of the system. Such a growth implies a consistent and homogeneous distribution of thermodynamic properties within the shell and reflects a stable configuration where the matter layers contribute regularly to the total entropy. The smooth increase of entropy with shell thickness therefore supports our charged model in a controlled and physically acceptable manner while maintaining regularity of the spacetime configuration.

4. Exterior space-time of gravastar

The interior smoothly matches the vacuum exterior at the surface at $r = R$ with the Reissner-Nordström spacetime in the exterior as stated by

$$\begin{aligned} ds^2 = & \left(1 - \frac{2M}{R} + \frac{q^2}{R^2}\right) dt^2 \\ & - \left(1 - \frac{2M}{R} + \frac{q^2}{R^2}\right)^{-1} dr^2 \\ & - r^2 \left(d\theta^2 + \sin^2\theta \, d\phi^2\right), \end{aligned} \tag{32}$$

where M is the mass of the gravitational system.

5. Junction condition and the EoS parameter

A gravastar is comprised of three regions: the interior, accompanied by the thin shell and the vacuum exterior. The shell functions as a bridge connecting the interior and the exterior geometry, thus serving as a pivotal part in the layout of the gravastar. A criterion was established for a smooth connection between the interior and the exterior geometries over the surface (Darmois [1927]; Misner & Sharp [1964]). The metric coefficients show continuous behavior at the

interface (here we take Σ at $r = D$) despite the fact that the derivatives of these metric coefficients may not be continuous there. The surface tension and the stress energy at the coupling interface can be inferred from the discontinuous change in the extrinsic curvature at the joining interface. We have the Lanczos' equation as

$$S_k^l = -\frac{1}{8\pi}(\xi_k^l - \delta_l^k \xi_k^k)\,, \tag{33}$$

where S_{ij} indicates the stress energy tensor. $\xi_{lk} = \gamma_{lk}^{+} - \gamma_{lk}^{-}$ reveals the extrinsic curvatures or rather the second fundamental form, with "+" and "−" indicating the interior and the exterior respectively. The second fundamental form bridging the interior and exterior boundaries of the thin shell are demonstrated as

$$\gamma_{\alpha\beta}^{\pm} = -n_{\mu}^{\pm}\left[\frac{\partial^2 X_{\mu}}{\partial\eta^{\alpha}\partial\eta^{\beta}} + \Gamma_{\sigma\tau}^{\mu}\frac{\partial X^{\sigma}}{\partial\eta^{\alpha}}\frac{\partial X^{\tau}}{\partial\eta^{\beta}}\right]|_{\Sigma}\,. \tag{34}$$

In the aforementioned expression, the intrinsic coordinates of the shell are characterized by η^{α}, and $n_{\mu}^{\pm}$ stand for the unit normals on the surface $\sum$ as given by

$$n_{\mu}^{\pm} = \pm\left|g^{ab}\frac{\partial f}{\partial X^a}\frac{\partial f}{\partial X^b}\right|^{-\frac{1}{2}}\frac{\partial f}{\partial X^{\mu}}\,, \tag{35}$$

where $n^k n_k = 1$, and $f(r)$ depicts the co-ordinate system for the exterior metric. Employing the Lanczos technique (Darmois [1927]), we can assess the surface stress energy tensor in the context of spherically symmetric space-time, as $S_{ij} = diag[\lambda, -\nu, -\nu, -\nu]$ where λ represents the surface energy density and ν is the surface pressure which are given by

$$\lambda = -\frac{1}{4\pi D}\left[\sqrt{f}\right]_{-}^{+} \tag{36}$$

and

$$\nu = -\frac{\lambda}{2} + \frac{1}{16\pi}\left[\frac{f'}{\sqrt{f}}\right]_{-}^{+}. \tag{37}$$

Using equations (20) and (32) in equation (36) we yield the following outcome

$$\lambda = -\frac{1}{4\pi D}\left[\sqrt{1 - \frac{2M}{D} + \frac{q^2}{D^2}} - \sqrt{1 - \frac{8\pi\rho_l D^2}{3} + \frac{\varkappa^2 D^{2m+2}}{2m+3}}\right]. \tag{38}$$

Figure 6 shows that the surface density maintains positivity over the surface region and increases gradually as it approaches the boundary of the shell for $\rho_l = 0.01$, $q = 1$ and $M = 3.35M_{\odot}$ which can potentially lead to negative surface pressure under certain conditions (Debnath [2021]). The figure also indicates that the shell contains physically acceptable matter and that

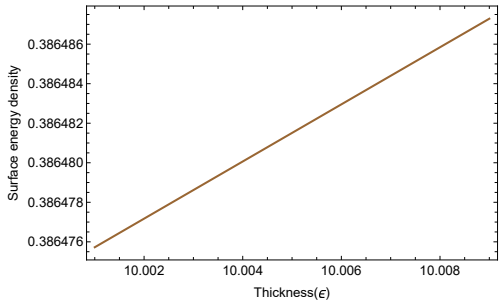

Fig. 6. Graph of the surface energy density with respect to the shell thickness (ϵ).

the surface energy distribution becomes more concentrated near the boundary. This gradual increase implies that the shell stores a larger fraction of its energy closer to the exterior interface. Under certain conditions, such a rise in surface density may lead to the development of negative surface pressure, which physically corresponds to a compressive stress acting along the shell surface. Using equations (20), (32) and (38) in equation (37) we get the surface pressure as

$$\nu = \frac{1}{8\pi D}\left[\sqrt{1-\frac{2M}{D}+\frac{q^2}{D^2}}-\sqrt{1-\frac{8\pi\rho_l D^2}{3}+\frac{\varkappa^2 D^{2m+2}}{2m+3}}\right] + \frac{1}{16\pi}\left[\frac{\frac{2M}{D^2}-\frac{2q^2}{D^3}}{\sqrt{1-\frac{2M}{D}+\frac{q^2}{D^2}}}-\frac{\left\{\frac{-16\pi\rho_l D}{3}+\frac{(2m+2)\varkappa^2 D^{2m+1}}{2m+3}\right\}}{\sqrt{1-\frac{8\pi\rho_l D^2}{3}+\frac{\varkappa^2 D^{2m+2}}{2m+3}}}\right]. \quad (39)$$

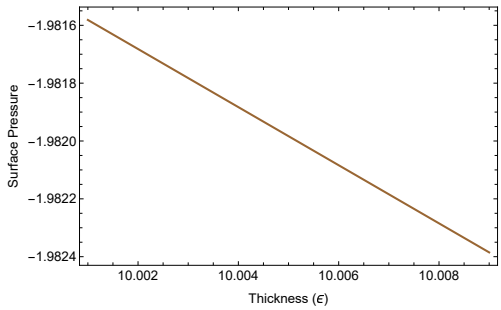

Fig. 7. Graph of the surface pressure with respect to the shell thickness (ϵ).

Figure 7 demonstrates the pressure distribution on the surface where it decreases with the increase in the radial co-ordinate but always keeps the

negative sign. Thus, the negative pressure might arise from the exotic matter in the shell (Debnath [2021]). The surface pressure represents the tangential stress acting along the shell. It is negative and decreases linearly to more negative values as the shell thickness increases, which physically indicates that the shell experiences surface tension. In gravitational systems, negative pressure corresponds to a compressive stress that acts to hold the shell together. The linear decrease towards more negative values suggests that as the shell becomes thicker, it strengthens the inward binding force within the shell. Physically, this behavior implies that the shell develops stronger cohesive stresses to counterbalance gravitational attraction and electromagnetic effects, thereby helping maintain the structural equilibrium of the gravastar configuration and preventing the collapse of the shell into a horizon or singular state. Using the equations (38) and (39) we have the EoS parameter as

$$w(D) = \frac{\nu}{\lambda} = -\frac{1}{2} - \frac{1}{4D} \frac{\left[\frac{\frac{2M}{D^2} - \frac{2q^2}{D^3}}{\sqrt{1-\frac{2M}{D}+\frac{q^2}{D^2}}} - \frac{\left\{\frac{-16\pi\rho_l D}{3} + \frac{(2m+2)\varkappa^2 D^{2m+1}}{2m+3}\right\}}{\sqrt{1-\frac{8\pi\rho_l D^2}{3}+\frac{\varkappa^2 D^{2m+2}}{2m+3}}}\right]}{\sqrt{1-\frac{2M}{D}+\frac{q^2}{D^2}} - \sqrt{1-\frac{8\pi\rho_l D^2}{3}+\frac{\varkappa^2 D^{2m+2}}{2m+3}}}. \tag{40}$$

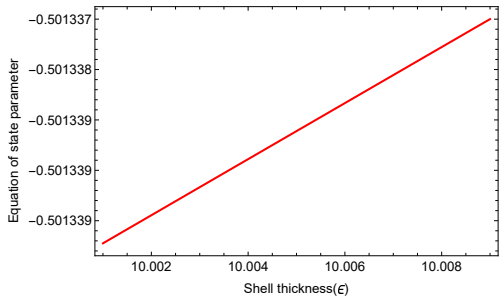

Fig. 8. Graph of the EoS parameter with respect to the shell thickness (ϵ).

From Fig. 8, we can say that the EoS parameter for the charged model increases with the increase in the radius and keeps the negative sign for $\rho_l = 0.01$, $q = 1$ and $M = 0.85M_\odot$ (Debnath [2021]). The EoS parameter characterizes the relationship between surface pressure and surface energy density of the shell matter. The plot in Fig. 8 for the EoS parameter indicates that the shell matter initially exhibits stronger negative pressure near the inner boundary, which gradually weakens as one moves outwards. Physically, a negative EoS parameter signifies the presence of repulsive or tension-dominated stresses that help counterbalance gravitational attraction within the shell. The linear increase toward less negative values implies that the magnitude of this tension decreases smoothly across the shell, suggesting a gradual transition of the matter properties from strongly tension-dominated behavior toward a less exotic

state near the outer boundary. This smooth and monotonic behavior also reflects a stable and physically consistent matter distribution within the shell. Consequently, we can compute the mass of the thin shell with the help of its surface density as

$$m_s = 4\pi D^2\lambda = -D\left[\sqrt{1-\frac{2M}{D}+\frac{q^2}{D^2}}-\sqrt{1-\frac{8\pi\rho_l D^2}{3}+\frac{\varkappa^2 D^{2m+2}}{2m+3}}\right]. \quad (41)$$

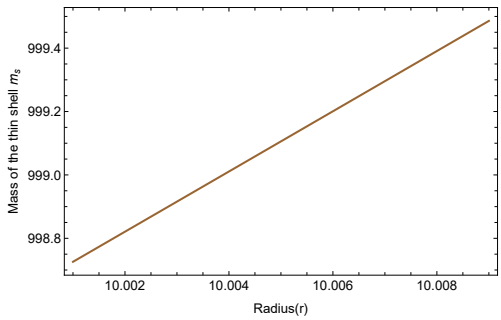

Fig. 9. Plot of the mass of the thin shell against the shell thickness (ϵ).

Figure 9 presents the thin shell mass' variation in regard to the thickness for the charged gravastar demonstrating that m_s is growing steadily with the increasing thickness which may necessitate the presence of exotic matter in the thin shell. The plot demonstrates that the total mass contribution grows steadily as the radial extent of the shell increases. The linear increase implies that the surface energy density contributes in a regular and nearly uniform manner across the shell. This behavior reflects a stable and well-distributed matter configuration across the shell, where the shell acts as the primary region responsible for maintaining a smooth and non-singular structure. Also, equation (41) gives us the gravastar's total mass as

$$\begin{aligned} M = \frac{1}{6D(2m+3)}\Big[& -3\varkappa^2 D^{2m+4} + 16\pi D^4\rho_l \\ & +6\sqrt{3}Dm_s\sqrt{\frac{3\varkappa^2 D^{2m+2}-16\pi D^2\rho_l m-24\pi D^2\rho_l+6m+9}{2m+3}} \\ & +4\sqrt{3}Dm_s m\sqrt{\frac{3\varkappa^2 D^{2m+2}-16\pi D^2\rho_l m-24\pi D^2\rho_l+6m+9}{2m+3}} \\ & 6q^2m+9q^2-6m_s^2m-9m_s^2\Big]. \end{aligned} \quad (42)$$

We can see clearly that once we have the values of $\varkappa$, m, the radial distance (D), the charge q and the mass of the thin shell, we can calculate the value of the total mass M.

6. Stability analysis and the boundary condition

Surface redshift studies are crucial for understanding the gravastar's stability and detection. The formula $Z_s = \frac{\lambda_0}{\lambda_e}$ facilitates the determination of a gravastar's surface redshift caused by the gravitational effects with λ_0 and λ_e signifying the observed and the emitted wavelengths. We have seen that the surface redshift of a stable and isotropic perfect fluid sphere cannot exceed 2 (Buchdahl [1959]; Straumann [1984]). It is also shown that $Z_s \leq 2$ for isotropic fluids when the cosmological constant is neglected (Barraco et al. [2002]). Here we have

$$Z_s = -1 + \sqrt{\frac{K + Cr^2}{K(1 + Cr^2)}}\,. \tag{43}$$

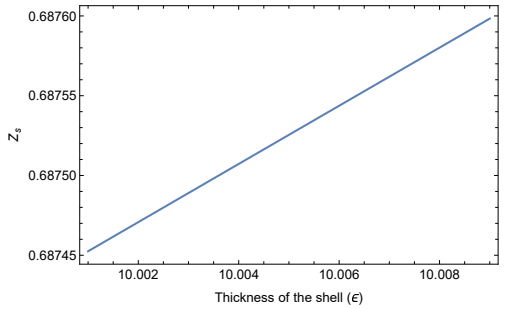

Fig. 10. Variation of the surface redshift parameter with respect to the shell thickness (ϵ).

Figure 10 presents the graphical representation of the surface redshift for our model. Thus, from the graph, under the consideration of Vaidya-Tikekar metric potential, we can see that the current gravastar model is stable and compatible as it stays well within the upper range of 1 and lower range 0 for $C = 0.003078799$ and $K = -1.313519$. The surface redshift measures the gravitational redshifting of light emitted from the shell due to the curvature of spacetime. Fig. 10 demonstrates that the gravitational field at the shell becomes gradually stronger as the shell becomes thicker, leading to a progressively larger redshift of the emitted radiation. The positive value confirms that photons lose energy while escaping the gravitational field of the configuration. At the same time, the fact that the redshift remains below unity implies that the gravitational field is moderate and does not approach the extreme regime associated with horizon formation. Physically, this behavior suggests that the shell contributes increasingly to the gravitational potential as its thickness grows, yet the configuration remains regular and stable, maintaining a well-behaved spacetime structure.

Conclusion

A key benefit of researching the gravastar objects is that it exhibit similarities with BHs. So far, no direct evidence of the existence of gravastars has been found. Nevertheless a few indirect indications are present in the literature to forecast the presence and potential future observation of the gravastar. A potential approach for detecting it was initially put forward by an exploration of gravastar shadows (Sakai et al. [2014]). An alternative approach for the identification of gravastars is the gravitational lensing method, in which it was asserted that in gravastar, micro-lensing consequences of enhanced peak luminosity in comparison to the BHs with masses of the same value could potentially happen (Kubo & Sakai [2016]). As stated in the references, apparently the ring-down signals observed through LIGO detectors of GW150914 are thought to be originated from objects lacking an event horizon, possibly resulting from a gravastar, although it remains unconfirmed so far (Abbott et al. [2016]; Cardoso et al. [2016a, 2016b]). In a recent analysis of the image obtained from First M-87 Event Horizon Telescope result, there is the possibility which cannot be ignored that the results could be attributed to a gravastar (EHT collaboration [2019]).

Here, our aim is to highlight a new solution of the charged gravastar model within the context of Einstein theory embracing the approach through Vaidya-Tikekar metric potential. It is comprised of a perfect fluid with charge and the spacetime continuum in the exterior is denoted by Reissner Nordström solution. In the wake of the gravastar model's proposal by Mazur and Mottola, a considerable amount of work has been done, and these cumulative evidences suggest that this gravastar model is acceptable, and it can address the challenges and flaws associated with BHs. In this article, we have covered the three regions of the postulated gravastar framework through its various distinctive attributes.

Interior region: By the application of the EoS $p = -\rho$ in the interior spacetime fabric, we have achieved a singularity free metric potential function. The core density ρ_l provides insights into pressure and density maintaining a constant value all over the inner region.

Intermediate Thin Shell: A layer of ultra-relativistic stiff fluid material characterized by the EoS $p = \rho$ has been examined in terms of its various characteristics such as the appropriate shell length and the thin shell's energy content together with its entropy. The variations of the metric potential $e^{y(r)}$ and the pressure-density w.r.t the thickness of the shell have been plotted in Figs. 1 and 2 where we can see that it maintains positivity and finiteness.

Figure 3 describes the relationship between the proper length of the shell and its thickness, how it increases with the thickness of the shell monotonically. Then, we have derived the expression for the energy content and the entropy within the shell and have graphically presented its variation as a function the thickness of the shell in Figs. 4 and 5. These results are all in agreement with other results of gravastar available in the literature (Das et al. [2017]; Debnath [2021]; Pradhan et al. [2023]).

Exterior spacetime: The exterior spacetime region of the charged model of the gravastar in vacuum is presented by the Reissner Nordström solution.

Additionally, we have also gone through the junction conditions for the smooth matching of our interior region with the exterior metric, with the thin

shell present at the interface between the two regions. It reveals that the shell is occupied with ultra-relativistic fluid adhering to the EoS $p = \rho$ and the material composition. In the context of the junction conditions we have derived the surface energy density and surface pressure. We have visualized from Fig. 6, that the surface density gradually increases as it approaches the outer vicinity. In Fig. 7, the surface pressure distribution is seen to be diminishing corresponding to an increase in shell thickness but it is always in negative region. In Fig. 8, we see the variation of the EoS parameter which increases with respect to the thickness (ϵ) and it is in the negative region. The variation of the mass of the thin shell is increasing with thickness as shown in Fig. 9 which implies the necessity of the thin shell's exotic matter content. And, we have executed a stability study for the charged gravastar model in our manuscript with the help of surface redshift. The physical viability of our gravastar model is presented in Fig. 10. Thus, we can draw a conclusion that we have endeavoured to portray a gravastar model from a different perspective taking the help of Vaidya-Tikekar metric potential. Our research has revealed that every solution is physically viable and stays non-singular at the origin. Therefore, this configuration of the model of the charged gravastar appears to be fairly reasonable and is worthy of further study.

References

Abbott B. P., et al., 2016, *Phys. Rev. Lett., 116, 061102.*
Abramowicz M. A., Kluzniak W., Lasota J. P., 2002, *Astron. Astrophys., 396, L31.*
Barraco D. E., et al., 2002, *Phys. Rev. D, 65, 124028.*
Berezin V., 2003, *Nucl. Phys. B, 661, 409.*
Bhar P., Rahaman F., Das S., Aktar S., Errehymy A., 2024, *Commun. Theor. Phys., 76, 015401.*
Bhattacharjee D., Chattopadhyay P. K., Paul B. C., 2023, *Phys. Dark Univ., 43, 101411.*
Bhattacharjee D., Chattopadhyay P. K., 2024, *J. High Energy Astrophys., 41, 100995.*
Bhatti M. Z., 2020, *Mod. Phys. Lett. A, 35, 2050069.*
Bhatti M. Z., Yousaf Z., Rehman A., 2020, *Phys. Dark Univ., 29, 100561.*
Biswas S., Shee D., Ray S., Rahaman F., Guha B. K., 2019, *Ann. Phys., 409, 167905.*
Blome J. J., Priester W., 1984, *Naturwissenschaften, 71, 528.*
Braje T. M., Romani R. W., 2002, *Astrophys. J., 580, 1043.*
Buchdahl H. A., 1959, *Phys. Rev., 116, 1027.*
Buchert T., 2001, *Gen. Relativ. Gravit., 33, 1381.*
Cardoso V., Franzin E., Pani P., 2016a, *Phys. Rev. Lett., 116, 171101.*
Cardoso V., Franzin E., Pani P., 2016b, *Phys. Rev. Lett., 117, 089902.*
Carmeli M., 1982, *Classical Fields: General Relativity and Gauge Theory, John Wiley and Sons, New York, 168–171.*
Carr B. J., 1975, *Astrophys. J., 201, 1.*
Carter B. M. N., 2005, *Class. Quantum Grav., 22, 4551.*
Chakraborty I., Pradhan A., 2001, *Grav. Cosmol., 7, 55.*
Chapline G., Hohlfeld E., Laughlin R. B., Santiago D. I., 2003, *Int. J. Mod. Phys. A, 18, 3587.*
Chirenti C. B. M. H., Rezzolla L., 2007, *Class. Quantum Grav., 24, 4191.*
Darmois G., 1927, *Mémorial des Sciences Mathématiques, Gauthier-Villars, Paris.*
Das A., Ghosh S., Guha B. K., Das S., Rahaman F., Ray S., 2017, *Phys. Rev. D, 95, 104014.*
Davies P. C. W., 1984, *Phys. Rev. D, 30, 737.*
de Felice F., Yu Y., Fang J., 1995, *Mon. Not. R. Astron. Soc., 277, L17.*
Debnath U., 2019, *Eur. Phys. J. C, 79, 1–9.*
Debnath U., 2021, *Eur. Phys. J. Plus, 136, 1–23.*
EHT Collaboration, 2019, *Astrophys. J. Lett., 875, L1.*
Einstein A., 1915, *Sitzungsberichte der Preussischen Akademie der Wissenschaften, Berlin.*
Errehymy A., Daoud M., 2021, *Eur. Phys. J. C, 81, 556.*
Errehymy A., Khedif Y., Daoud M., 2021, *Eur. Phys. J. C, 81, 266.*

Errehymy A., Mustafa G., Khedif Y., Daoud M., Alrebdi H. I., 2022, *Eur. Phys. J. C, 82, 1023*.
Ghosh S., Rahaman F., Guha B. K., Ray S., 2017, *Phys. Lett. B, 767, 380–385*.
Ghosh S., Shee D., Ray S., Rahaman F., Guha B. K., 2020, *Results Phys., 17, 103131*.
Ghosh S., Dey S., Das A., Chanda A., Paul B. C., 2021, *J. Cosmol. Astropart. Phys., 2021, 004*.
Gliner E. B., 1966, *Sov. Phys. JETP, 22, 378*.
Gupta Y. K., Maurya S. K., 2011, *Astrophys. Space Sci., 331, 135–141*.
Hogan C., 1984, *Nature, 310, 365*.
Ilyas M., Athar A. R., Bibi A., 2023, *New Astron., 103, 102053*.
Islam J. N., 1985, *Rotating Fields in General Relativity, Cambridge University Press, Cambridge and New York*.
Kaiser N., Stebbins A., 1984, *Nature, 310, 391*.
Kubo T., Sakai N., 2016, *Phys. Rev. D, 93, 084051*.
Kumar J., Prasad A. K., Maurya S. K., Banerjee A., 2018, *Eur. Phys. J. C, 78, 540*.
Linares L. P., Malheiro M., Ray S., 2004, *Int. J. Mod. Phys. D, 13, 1355*.
Lohakare S. V., Maurya S. K., Singh K. N., Mishra B., Errehymy A., 2022, *Mon. Not. R. Astron. Soc., 512, 1507–1517*.
Madsen M. S., Mimoso J. P., Butcher J. A., Ellis G. F. R., 1992, *Phys. Rev. D, 46, 1399*.
Maurya S. K., Gupta Y. K., Ray S., Dayanandan B., 2015, *Eur. Phys. J. C, 75, 225*.
Maurya S. K., Govender M., 2017, *Eur. Phys. J. C, 77, 347*.
Maurya S. K., Govender M., et al., 2019, *Eur. Phys. J. C, 79, 85*.
Maurya S. K., 2020, *Eur. Phys. J. C, 80, 429*.
Maurya S. K., Tello-Ortiz F., 2020a, *Ann. Phys., 414, 168098*.
Maurya S. K., Tello-Ortiz F., 2020b, *Phys. Dark Univ., 27, 100442*.
Maurya S. K., Errehymy A., Daoud M., Govender M., 2022, *Fortschr. Phys., 70, 2200031*.
Maurya S. K., Errehymy A., Govender M., Jasim M. K., Al-Harbi N., 2023, *Eur. Phys. J. C, 83, 348*.
Maurya S. K., Errehymy A., Jasim M. K., Daoud M., Al-Harbi N., 2023, *Eur. Phys. J. C, 83, 317*.
Maurya S. K., Jasim M. K., Errehymy A., Nisar K. S., Mahmoud M., Nag R., 2023, *Fortschr. Phys., 71, 2300025*.
Maurya S. K., Mustafa G., Ray S., Dayanandan B., Aziz A., Errehymy A., 2023, *Phys. Dark Univ., 42, 101284*.
Maurya S. K., Errehymy A., Jasim M. K., Daoud M., Al-Harbi N., 2024, *Prog. Theor. Exp. Phys., 2024, 063E01*.
Maurya S. K., Errehymy A., Umbetova Z., Jasim M. K., Daoud M., Al-Harbi N., 2025, *J. High Energy Astrophys., 45, 100391*.
Mazur P. O., Mottola E., 2001, *LA-UR-01-5067*.
Mazur P. O., Mottola E., 2004, *Proc. Natl. Acad. Sci. USA, 101, 9545*.
Mielke E. W., Schunck F. E., 2000, *Nucl. Phys. B, 564, 185*.
Misner C. W., Sharp D., 1964, *Phys. Rev., 136, B571*.
Mohanty D., Ghosh S., Sahoo P. K., 2023, *Ann. Phys., 452, 169297*.
Mohanty D., Ghosh S., Sahoo P. K., 2024, *Phys. Dark Univ., 44, 101470*.
Mustafa G., Javed F., Maurya S. K., Waseem A., Fatima G., 2024, *Phys. Dark Univ., 45, 101515*.
Naz S., Sharif M., 2022, *Universe, 8, 142*.
Övgün A., Sert Ö., Adak M., 2017, *Eur. Phys. J. C, 77, 105*.
Pradhan S., Mandal S., Sahoo P. K., 2023, *Chin. Phys. C, 47, 055103*.
Pradhan S., Mohanty D., Sahoo P. K., 2023, *Chin. Phys. C, 47, 095104*.
Rahaman F., Ray S., Usmani A. A., Islam S., 2012, *Phys. Lett. B, 707, 319–322*.
Ray S., Sengupta R., Nimesh H., 2020, *Int. J. Mod. Phys. A, 35, 2050076*.
Rej P., Errehymy A., Daoud M., 2023, *Eur. Phys. J. C, 83, 392*.
Sakai N., Saida H., Tamaki T., 2014, *Phys. Rev. D, 90, 104013*.
Sanjay T., Narasimhamurthy S. K., Nekouee Z., 2024, *Eur. Phys. J. C, 84, 393*.
Schwarzschild K., 1916, *Sitzungsberichte der Königlich Preussischen Akademie der Wissenschaften, Berlin, 18*.
Shafeek A. T., Bakry M. A., Moatimid G. M., 2023, *Pramana, 97(4), 189*.
Sharif M., Waseem A., 2019, *Astrophys. Space Sci., 364, 189*.
Sharif M., Saeed M., 2022, *Chin. J. Phys., 77*.
Sinha M., Singh S. S., 2025a, *Ann. Phys., 480, 170129*.
Sinha M., Singh S. S., 2025b, *Int. J. Mod. Phys. A, 40, 2550043*.
Stephens C. R., 't Hooft G., Whiting B. F., 1994, *Class. Quantum Grav., 11, 621*.

Straumann N., 1984, *Gen. Relativ. Astrophys., Springer, Berlin.*
Vaidya P. C., Tikekar R., 1982, *J. Astrophys. Astro., 3, 325.*
Visser M., Wiltshire D. L., 2004, *Class. Quantum Grav., 21, 1135.*
Yousaf Z., Bamba K., Bhatti M. Z., Ghafoor U., 2019, *Phys. Rev. D, 100, 024062.*
Zel'dovich Y. B., 1972, *Mon. Not. R. Astron. Soc., 160, 1.*